

# High-Purity Er<sub>3</sub>N@C<sub>80</sub> Films: Morphology, Spectroscopic Characterization, and Thermal Stability

Jürgen Weippert, Seyithan Ulaş, Patrick Per Meyer, Dmitry V. Strelnikov, and Artur Böttcher\*

Films comprising the endohedral fullerene Er<sub>3</sub>N@C<sub>80</sub> are deposited onto highly oriented pyrolytic graphite (HOPG) substrates in high purity enabled by performing mass-selected low-energy deposition from a cation beam. In the initial stage, the growth on HOPG is dominated by spontaneous nucleation of small 2D islands both on intact terraces as well as the step edges. The island growth exhibits strong differences from films comprising other fullerenes grown by the same method. This behavior can be explained by the surface-diffusion-mediated nucleation model presented in previous work: Dominant components in the behavioural differences are a high intercage dispersion interaction and a lower kinetic energy of cages migrating on the surface in comparison with previously deposited materials. When annealed, the films undergo several competing processes: A small fraction desorbs in the temperature range 700–800 K, another fraction forms covalent intercage bonds instead of the previous purely dispersive bonding mode, and a third fraction probably decomposes to small fragments.

corresponding oxide Ln<sub>2</sub>O<sub>3</sub> and introducing nitrogen via the gas phase.<sup>[3,6]</sup>

Whereas many endohedral fullerenes, especially those with a pure nonmetallic interior, decompose upon thermal treatment,<sup>[7,8]</sup> Er<sub>3</sub>N@C<sub>80</sub> has been found to be sublimable.<sup>[9]</sup> Due to the lanthanide atoms, NCFs have unique magnetic properties<sup>[10–14]</sup> and also exhibit interesting absorption and luminescence properties<sup>[15,16]</sup> making them a potential material for photonic crystals.<sup>[17]</sup>

In this work, Er<sub>3</sub>N@C<sub>80</sub> was chosen as a building block for the growth of solid films. Its molecular structure is shown in **Figure 1**. The cage structure does not correspond to the structure of isolated C<sub>80</sub> of which two isomers with D<sub>2</sub><sup>[18–21]</sup> and D<sub>5d</sub><sup>[22]</sup> symmetries have been isolated. Instead the cage has an I<sub>h</sub> symmetry,<sup>[23,24]</sup>

which according to density functional theory (DFT) calculations is the most stable structure of C<sub>80</sub><sup>[25,26]</sup>. Recently, a less abundant isomer with D<sub>5h</sub> symmetry<sup>[27]</sup> has also been isolated. By magnetic analysis<sup>[13]</sup> fluorescence measurements,<sup>[28]</sup> the lanthanide charge state has been verified as Er<sup>3+</sup>. In contrast to other heavy lanthanide NCFs such as Gd<sub>3</sub>N@C<sub>80</sub><sup>[29]</sup> (of which even an isomer violating the isolated pentagon rule<sup>[30]</sup> (IPR) has been isolated<sup>[31]</sup>) and Tb<sub>3</sub>N@C<sub>80</sub>,<sup>[32]</sup> the Er<sub>3</sub>N cluster is almost planar and the Er atoms are oriented toward three hexagons in the cage. Its orientation has been found to be rather affixed in contrast to nitrideless lanthanide encapsulations, which have shown a more dynamic behavior.<sup>[25]</sup> The overall cross-section of the cage in comparison with the empty homologue has been found to increase by just 0.1%<sup>[33]</sup>. In bulk crystals, the cages assume an fcc packed structure.<sup>[34]</sup>

In the last two decades we routinely applied the low-energy cluster beam deposition technique (LECBD) to grow monodispersed IPR (C<sub>60</sub>, C<sub>70</sub>) and non-IPR (C<sub>58</sub> – C<sub>48</sub> and C<sub>68</sub> – C<sub>62</sub>) fullerene films.<sup>[35–37]</sup> The study of the film growth and thermal stability has proven to be a valuable way to explore the interaction and possible reactions between the cages with respect to their structure. In the unique case of the non-IPR fullerenes the morphology of the films is primarily governed by the ability of the gently landed cages to form covalent intercage C–C bonds bridging the nearest non-IPR sites. Despite this dominating process, LE CBD offers an important advantageous property: The morphology of the films can be tuned by varying 1) the kinetic energy of impinging cages, 2) the excitation

## 1. Introduction

Among endohedral fullerenes, defined as fullerene cages with encapsulated heteroatoms, lanthanide metal nitrogen cluster fullerenes (NCFs) Ln<sub>3</sub>N@C<sub>80</sub> hold a special position. They can be synthesized in relatively high yields<sup>[1–3]</sup> compared to other endohedral species<sup>[4]</sup> using conventional Krätschmer–Huffman generators<sup>[5]</sup> by doping the primary graphite material with the

Dr. J. Weippert, Dr. S. Ulaş, P. P. Meyer, Dr. D. V. Strelnikov, Dr. A. Böttcher  
Microscopic Systems Division  
Institute of Physical Chemistry  
KIT  
Karlsruhe 76131, Germany  
E-mail: artur.boettcher@kit.edu

Dr. J. Weippert  
Fraunhofer IAF  
Fraunhofer Institute for Applied Solid State Physics  
Freiburg 79108, Germany

 The ORCID identification number(s) for the author(s) of this article can be found under <https://doi.org/10.1002/pssb.202000546>.

© 2021 The Authors. Physica status solidi (b) basic solid state physics published by Wiley-VCH GmbH. This is an open access article under the terms of the Creative Commons Attribution-NonCommercial-NoDerivs License, which permits use and distribution in any medium, provided the original work is properly cited, the use is non-commercial and no modifications or adaptations are made.

DOI: 10.1002/pssb.202000546

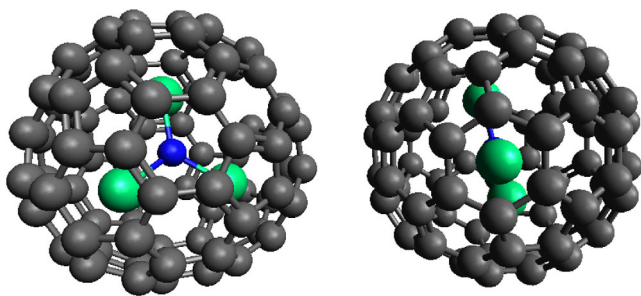


**Figure 1.** Structure of  $\text{Er}_3\text{N}@I_h\text{-C}_{80}$ <sup>[23,24]</sup>. The cage itself has an  $I_h$  symmetry, whereas the  $\text{Er}_3\text{N}$  cluster is almost planar and oriented towards three hexagons.

energy of the fullerene ion, and 3) the surface temperature.<sup>[38]</sup> In this context it is also a question of interest to verify that endohedral fullerenes with encapsulated material can be deposited with this technique intactly and to explore eventual differences in the growth mode with regard to the already investigated species.

## 2. Experimental and Computational Details

To achieve maximal purity in the deposited films, the film preparation was performed in the LECBD setup, which has been described before.<sup>[39]</sup> The  $\text{Er}_3\text{N}@C_{80}$  source material (LUNA Innovations [TrimetaspHERE] or SES Research, 95–97%) was sublimed at a temperature range of 900–1200 K building on experiments by Stibor et al.<sup>[9]</sup> The resulting neutral molecular beam was subsequently ionized by electron impact ionization (impact energy  $\approx 70$  eV). For more details on the sublimation process and the ion source, please refer to the Supporting Information. From the mixed ion/neutral molecular beam, cations were selected by means of a quadrupole bender. The desired species was selected by a quadrupole mass filter (Extrel Merlin, 1–4000  $\mu$ ) and finally directed to the substrate, at which a retarding potential was applied to ensure “soft-landing” conditions (impact energy  $\approx 6$  eV). As substrates highly oriented pyrolytic graphite (HOPG, SPI supplies, SPI-2 grade equivalent to ZYB) and gold substrates for surface enhanced Raman spectroscopy (SERS, Klarite) were used. HOPG was chosen as a substrate as it is conducting and rather inert and is a tried and tested substrate for fullerene film growth with this particular method.<sup>[35–37,39]</sup> The nominal coverage was determined by integrating the ion current; it has previously been determined<sup>[35]</sup> that in this setup 20 nAmin of fullerenes corresponds to 1 monolayer (ML) equivalent.

The samples were characterized in situ by ultraviolet photoelectron spectroscopy (UPS, Thermo VG Scientific UVL-HI-384 radiation source with 21.22 eV, Omicron EA 125 energy analyzer), X-ray photoelectron spectroscopy (XPS, Omicron DAR-400 Mg K $\alpha$  radiation source with 1253.6 eV, same analyzer), Raman spectroscopy (Kaiser Optical Systems RXN1, Invictus Excitation Laser, 785 nm), and temperature programmed desorption spectroscopy (TPD, FHI-ELAB GO74 temperature controller and detection by Extrel Merlin mass filter, 1–4000  $\mu$ ). Atomic force microscopy (AFM) was performed ex situ (Autoprobe CP2, Veeco Instruments with HALCYONICS Micro 40 drive unit).

TPD spectra were analyzed using the Redhead equation<sup>[40]</sup>

$$E_A/RT_p = \ln\left(\frac{\nu_1 T_p}{\beta}\right) - 3.64 \quad (1)$$

To determine the desorption activation energy  $E_A$  from the desorption rate maximum temperature  $T_p$  at a certain heating rate  $\beta$ , the  $C_{60}$  frequency factor  $10^{13.2}$  Hz<sup>[41]</sup> was used.

DFT calculations – geometry optimization and harmonic vibrational analysis<sup>[42]</sup> – were performed using Turbomole<sup>[43,44]</sup> with the BP86 functional<sup>[45,46]</sup> and the def2-SVP basis set<sup>[47]</sup> in RI approximation.<sup>[48]</sup> This level of theory has been proven to provide good agreement between theoretical and experimental vibrational spectra of neutral and charged fullerenes before<sup>[49,50]</sup> with mild redshifts for wavenumbers  $< 700$   $\text{cm}^{-1}$  and small blueshifts for wavenumbers  $> 1300$   $\text{cm}^{-1}$ . Raman intensities were calculated both in a static and dynamic polarizability approach.<sup>[51]</sup>

## 3. Results and Discussion

### 3.1. Characterization of the as-Prepared Films

$\text{Er}_3\text{N}@C_{80}$  films of various thicknesses were deposited at room temperature (RT). To explore cage–cage and cage–surface interactions, we compared the morphology of the  $\text{Er}_3\text{N}@C_{80}$  films to the well-known IPR fullerene  $C_{60}$  and the best-studied non-IPR fullerene  $C_{58}$  upon whose film growth numerous works have been published (see refs. [38,52,53]).

**Figure 2A** shows the representative topography of a 1 ML thick  $C_{60}$  film comprising IPR- $I_h\text{-C}_{60}$  cages, exclusively. The surface topography is dominated by planar round islands ( $\approx 1$  cage high) pinned by the step edges of the substrate. The second  $C_{60}$  layer starts to grow before the completion of the first layer. Small dendritic islands appear on top of the  $C_{60}(111)$  islands of the first layer. This scenario has been explained by different corrugations of the involved surfaces,  $C(001)$  and  $C_{60}(111)$ , which govern the surface mobility of the adsorbed cages.<sup>[52]</sup> The growth of planar compact islands of the first layer results from extremely low diffusion and rotation barriers (13 and 28 meV, respectively), which critically facilitate the surface mobility of the  $C_{60}$  cages at room temperature at which the thermal energy  $k_B T$  corresponds to 26 meV.<sup>[54]</sup> The binding energy of a  $C_{60}\text{-}C_{60}$  dimer is lower than 270 meV; that is, a cage terminating the rim via a single van der Waals (vdW) bond can be easily decoupled from the periphery already at room temperature. It migrates as long as it gets stabilized by a higher coordinated adsorption site in the already formed  $C_{60}$  network. When a cage adsorbs on top of a densely packed  $C_{60}(111)$  island, its surface mobility is significantly hindered by the high diffusion barrier of 168 meV<sup>[54]</sup> and consequently rather dendritic islands grow. Thus, this growth mode originates from the differences in the diffusion barriers for an IPR cage on  $C(001)$  and  $C_{60}(111)$  surfaces.

The growth of islands consisting of non-IPR fullerene cages differs substantially from that shown in **Figure 2A** for IPR- $C_{60}$  films.<sup>[35]</sup> The growth modes of  $C_{58}$  islands on HOPG were studied in detail by combining AFM, STM, XPS, UPS, and Raman spectroscopy.<sup>[38]</sup> All these studies commonly exposed the role of the adjacent pentagon motifs governing the reactivity of the carbon cages. The most stable  $C_{58}$  cage has a  $C_{3v}$  symmetry and

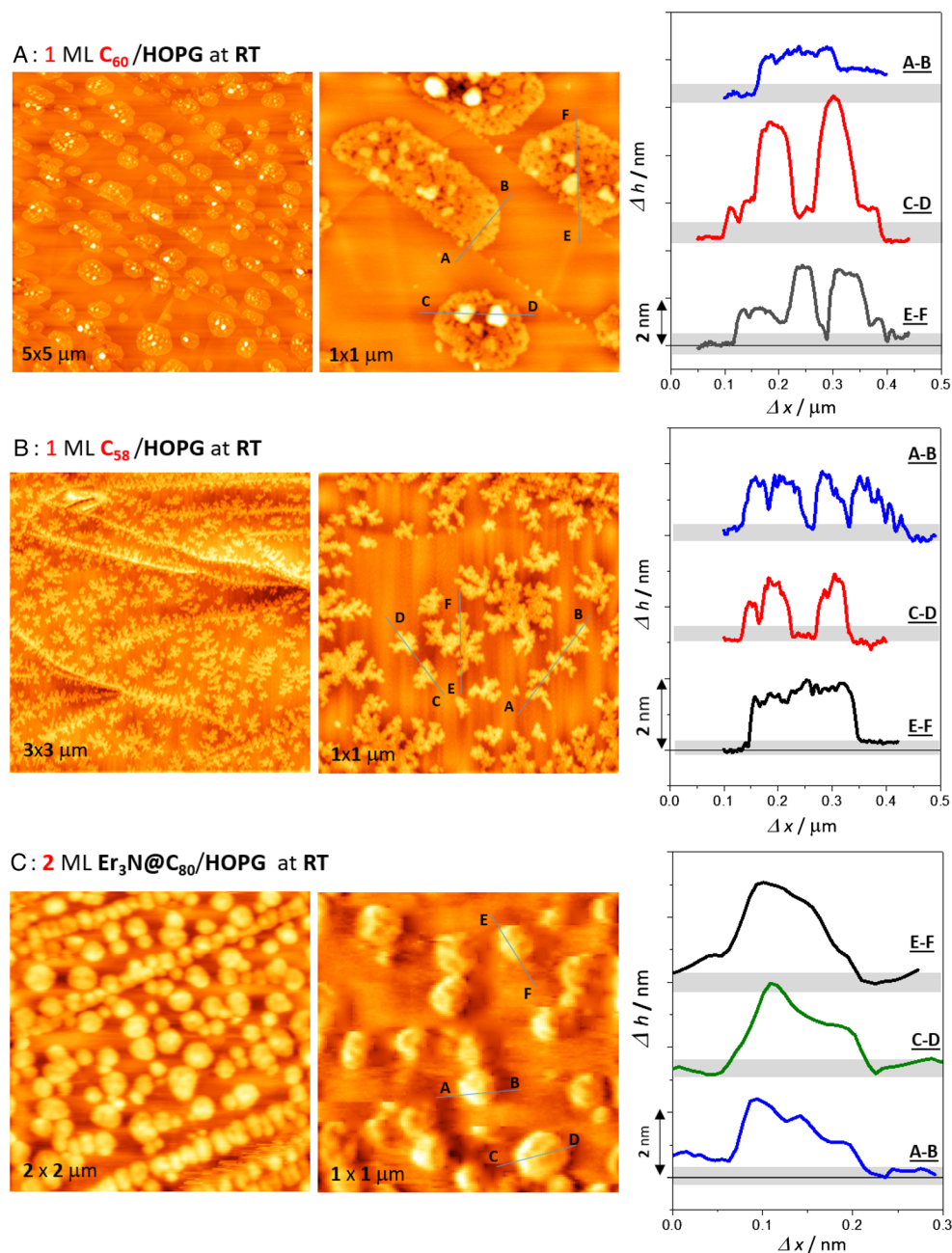


**Figure 2.** Comparison of AFM micrographs of untreated fullerenes deposited onto HOPG at room temperature. A)  $C_{60}$ ; B)  $C_{58}$ ; and C)  $Er_3N@C_{80}$ .

exhibits six isolated and three adjacent pentagon sites. These cages may form bonds both via vdW interaction and via polymerization that may occur both directly at the adjacent pentagon site and in its vicinity.<sup>[37]</sup> Figure 2B shows one example illustrating the initial growth stage of  $C_{58}$  islands on HOPG. All imperfections in the basal plane are more reactive than the  $sp^2$ -hybridized network of the graphene layer and consequently act as pinning sites where the nucleation of small 2D- $C_{58}$  islands onsets. A sticking of  $C_{58}$  to an undefected basal plane has never been observed. The growth of the dendritic  $C_{58}$  islands has been attributed to the formation of covalent intercage bonds that are

mediated by thermal surface diffusion.<sup>[38]</sup> Due to the importance of the latter, the dissipative conversion of the impact energy of an ion impinging from the gas phase into translational energy perpendicular to the surface is a crucial factor for the film growth.

Figure 2C shows the topography of a 2 ML  $Er_3N@C_{80}$  film. In contrast to the expectations, the topography of the  $Er_3N@C_{80}$  islands differs essentially from that we found for  $I_h-C_{60}$  islands discussed earlier and from  $Er_3N@C_{80}$  on metal surfaces<sup>[55,56]</sup> for which flat densely packed films had been observed. Already at very initial growth stages the flat terraces are decorated by

compact 3D islands (average 4 nm height and <200 nm width). One cannot distinguish between one monolayer high 2D smooth-rimmed islands and some dendritic islands in the second layer. Moreover, in contrast to  $I_h$ - $C_{60}$  films, for which the islands grown are pinned by the step edges, the majority of the  $Er_3N@C_{80}$  aggregates are randomly distributed over the flat terraces. The mean lateral density of the islands of  $\approx 25 \mu m^{-2}$  depends only slightly on the width of the terraces. The mean distance between the adjacent islands of <200 nm compares roughly with the mean free diffusion length.<sup>[38]</sup> This finding indicates that in comparison with  $C_{60}$  a smaller fraction of the impact energy of the impinging ions is converted into translational energy. The formation of compact, clod-like aggregates as observed in later growth stages demonstrated by the topographies of thick  $Er_3N@C_{80}$  films in **Figure 3** confirms a high interaction energy between the cages that was observed for other NCFs.<sup>[57]</sup>

On films with various multilayer coverages, UPS were acquired. A representative example along with the theoretical density of states (DOS) can be found in **Figure 4**. It has the usual shape of a fullerene UPS<sup>[36,58]</sup>. The binding energy range 4–9 eV consists of a series of strong, broad features, whereas the range 0–4 eV contains some weaker but highly cage-specific emission peaks. The spectrum is in good agreement with the DOS; note that if  $Er_3N@C_{80}$  was deposited directly from an effusion source without the mass spectrometric purification (see Supporting Information), this quality of agreement would not be achieved and would require extensive additional chromatographic purification otherwise.<sup>[59,60]</sup> In a more detailed theoretical work by Tang et al.<sup>[61]</sup> on the BLYP/DNP–DFT level<sup>[62–64]</sup> additionally a partial DOS of  $Er_3N$  has been calculated. It shows that the cluster has its major direct contributions to the DOS in the binding energy range of 6–10 eV. At lower binding energies, the major contribution to differences from UPS of pure  $C_{80}$  (see Supporting Information and Cummins et al.<sup>[19]</sup>), therefore, results from the different cage symmetry that is caused by the negative charge on the carbon grid.

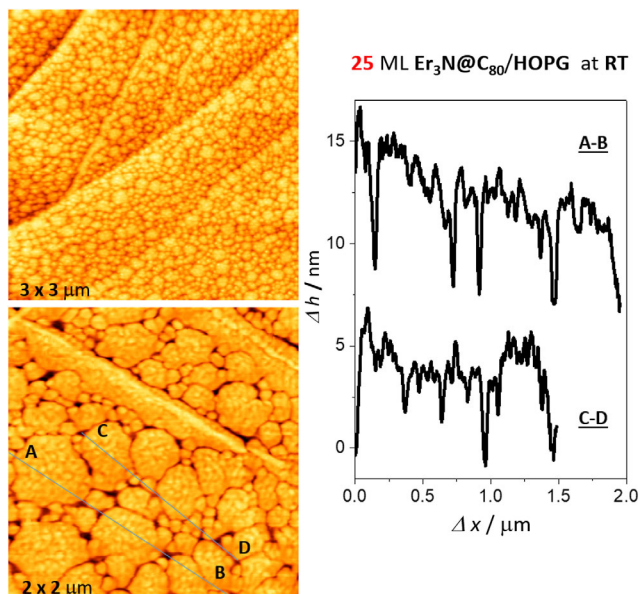


**Figure 3.** AFM micrographs of an untreated thick  $Er_3N@C_{80}$  film with a clod-like surface topography on HOPG.

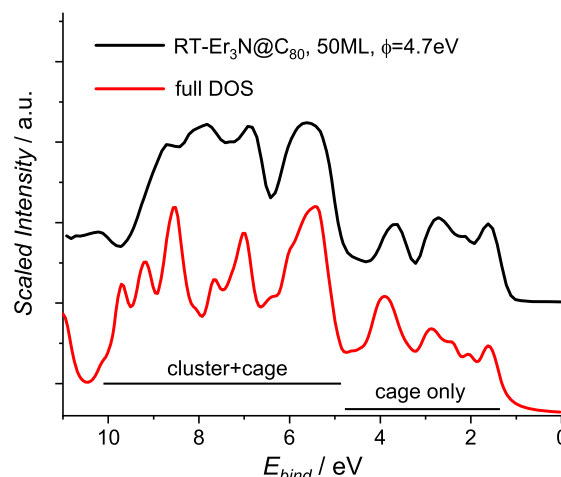


**Figure 4.** UPS of an untreated, 50 ML thick  $Er_3N@C_{80}$  film on HOPG in good agreement with a DFT-calculated DOS. According to Tang et al.<sup>[61]</sup> direct photoemission from the cluster takes place at binding energies >6 eV, whereas smaller binding energies are dominated by emission from the cage.

The vibrational structure of  $Er_3N@C_{80}$  has been explored by SERS in comparison with Raman spectra of the bulk powder. In **Figure 5A** experimental as well as calculated Raman spectra are shown. The powder spectra exhibited a strong luminescent background, which heavily lowered the signal-to-noise ratio. In the Supporting Information, a table of all reproducible SERS peaks, the unsubtracted bulk powder spectrum, and a Molden file for the visualization of all calculated vibrations can be found.

At low wavenumbers, the first apparent feature in SERS is three well-separated bands at 229, 260, and 295  $cm^{-1}$  which also occur in the bulk spectra at the identical positions. As **Figure 5B** shows, both calculation methods reconstruct these bands decently with the aforementioned redshift<sup>[49,50]</sup> which in this range amounts to 11  $cm^{-1}$ . All three bands correspond to strong cage deformation vibrations in which the cluster moves along with the surrounding carbon atoms; for the 229  $cm^{-1}$  band this cluster motion is the strongest. Raman measurements on other NCFs<sup>[65]</sup> have shown a single dominating band, which has been assigned to an out-of-plane  $\delta_{Er-N-Er}$  vibration of the cluster. Here, neither the experimental nor the theoretically calculated spectra show a pronounced  $\delta$  band; it only appears as a side feature in the dynamic calculation. In the bulk spectrum there is a minor elevation in the area of 275  $cm^{-1}$ , but it does not suffice for the assignment of a  $\delta$  peak.

Up to 900  $cm^{-1}$ , radial vibrations of the cage are dominant. It has to be remarked that in contrast to  $Sc_3N@C_{80}$ , which has exhibited a single pronounced symmetric  $\nu_{s,Er-N}$  stretching vibration<sup>[65]</sup> our calculations show that in the region 350–500  $cm^{-1}$  there are actually multiple vibrational modes consisting of a strong radial motion in the form of multiple wave packets migrating along the grid while the cluster performs a weak symmetric motion. The modes in the region 500–900  $cm^{-1}$  are also radial but involve simultaneous motion of all cage atoms with a weaker amplitude than in the previous group; among these, a band at 672  $cm^{-1}$  is the most pronounced one, which in FTIR

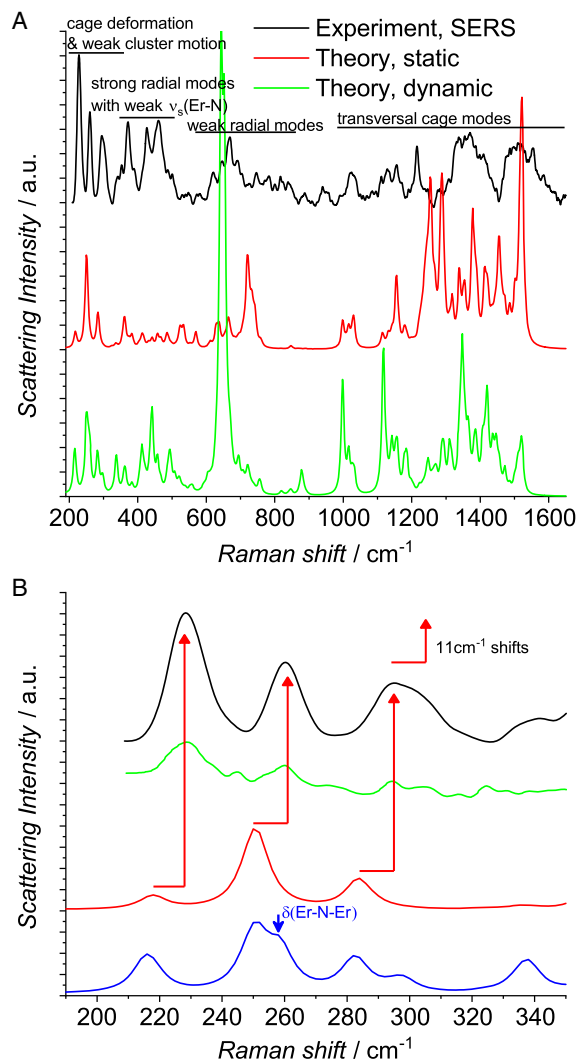


**Figure 5.** Experimental and theoretically calculated Raman spectra; black line: SERS of 0.25 ML  $\text{Er}_3\text{N}@C_{80}$ ; green line: bulk powder (impure); red line: static polarizability calculation; blue line: dynamic polarizability calculation. A) full spectral range with general peak assignments; B) detailed view of low wavenumbers.

spectra<sup>[66–68]</sup> has been observed as a side component of the anti-symmetric stretching vibration  $\nu_{\text{as,Er-N}}$  at  $703\text{ cm}^{-1}$ .

In the range  $1000\text{--}1600\text{ cm}^{-1}$ , transversal modes of the cage that consist of various combinations of ring breathing can be found.

In summary, the vibrational analysis has shown a significant difference in comparison with other  $M_3\text{N}@C_{80}$  fullerenes as pronounced peaks correlated to pure cluster vibrations as the  $\delta$  or a single  $\nu_{\text{s,Er-N}}$  peak was not observed. Now that the RT state of the films is well characterized, let us consider high-temperature (HT) effects.

### 3.2. Investigations of Thermally Induced Effects

Films of various thicknesses on HOPG were annealed to 1100 K. In **Figure 6a** temperature programmed desorption (TPD) for a

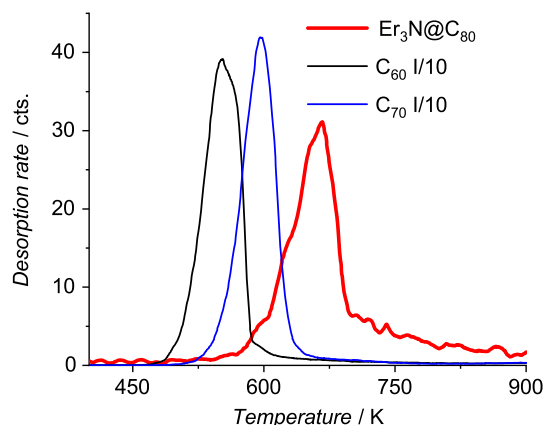


**Figure 6.** TPD spectrum of 0.2 ML  $\text{Er}_3\text{N}@C_{80}$  from HOPG;  $\beta = 4.25\text{ K s}^{-1}$  in comparison with coverage normalized spectra of  $C_{60}$  and  $C_{70}$ . The  $\text{Er}_3\text{N}@C_{80}$  peak maximum of 667 K corresponds to a desorption energy of 1.83 eV.

thin submonolayer film is shown. In order to avoid issues due to the transmission of the analyzer (see supplement of ref. [37]), we measured the intensity of  $\text{Er}_3\text{N}@C_{80}^{2+}$ , which is expected to be similar to the single charged species<sup>[9]</sup> at our settings. The desorption takes place around a maximum of 667 K, which is 110 K higher than for  $C_{60}$  (see also Ulbricht et al. and Weippert et al.<sup>[37,41]</sup>) and 70 K higher than for  $C_{70}$ . A Redhead analysis provides a binding energy of 1.83 eV, which is 0.3 eV higher than the energy of  $C_{60}$  and 0.2 eV higher than that of  $C_{70}$ . This reflects the aforementioned stronger dispersive interaction of  $\text{Er}_3\text{N}@C_{80}$ ; however, a single-shot desorption spectrum of  $C_{80}$  (see Supporting Information) has its peak in a similar temperature range, which indicates that the binding energy increase is mostly due to the cage size. It is also worth mentioning that the overall desorption intensity is a factor of 5 lower than it would be for a corresponding  $C_{60}$  film in our setup. This indicates that the desorption is not complete and a large fraction of the film goes to other process channels.

Some of these channels can be explored by AFM (see **Figure 7**) and photoelectron spectroscopy (**Figure 8**). **Figure 7** shows the AFM topography of initially 2 and 50 ML thick  $\text{Er}_3\text{N}@C_{80}$  films after annealing the sample up to 1100 K. As expected from the TPD experiments, the heating procedure applied does not remove all the deposited material. The step edges that pinned large  $\text{Er}_3\text{N}@C_{80}$  islands in the as-prepared samples are now decorated by differently shaped aggregates of 4–8 nm height and 100–200 nm width. Note that the size of the aggregates does not depend on the initial coverage  $\theta_0$  and different sizes can be observed in identical samples. In contrast to the as-prepared samples the flat terraces that were covered are now completely empty. Thus, the thermal treatment applied here removed all the material stored on the terraces and considerably modified the aggregates pinned by the step edges. The surface topography of the HT samples resembles features we observed when applying the same thermal treatment to thin fullerene films consisting of non-IPR- $C_{60}$  cages and we found spectral evidence for the thermally activated fusion of the cages at step edges.<sup>[69]</sup> We observed nearly the same AFM topography of the surface created by

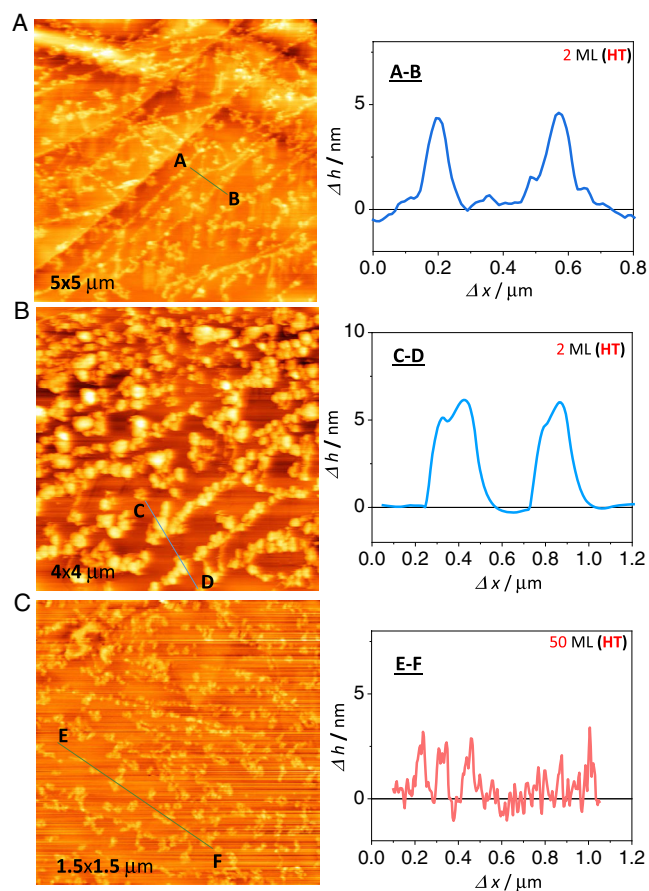


**Figure 7.** AFM micrographs of  $\text{Er}_3\text{N}@C_{80}$  films on HOPG after annealing to 1100 K. A)  $\theta_0 = 2$  ML with narrower aggregates; B)  $\theta_0 = 2$  ML with broader aggregates; C)  $\theta_0 = 50$  ML with aggregates that are not higher than in the  $\theta_0 = 2$  ML case.

heating thin  $C_{58}$  films deposited by LECBD on HOPG.<sup>[37]</sup> The  $C_{58}$  aggregates covalently pinned by step edges (surviving the HT treatment) were identified as oligomers consisting of fused or/and multifold covalently interlinked  $C_{58}$  cages. Yet, we have to acknowledge the possibility that these aggregates are not fused but rather debris that resulted from the cages cracking in a similar manner as  $\text{N}@C_{60}$  does<sup>[7]</sup> at elevated temperatures.

As the surface is not free of coverage, the UPS (Figure 8A) of HT  $\text{Er}_3\text{N}@C_{80}$  does not revolve to the original HOPG shape and even exhibits a significant DOS at the Fermi level, which indicates that the fusion products or debris are metallically conducting. An XPS analysis of  $\text{Er}4d$  (Figure 8B) provides further insight: RT  $\text{Er}_3\text{N}@C_{80}$  exhibits a typical  $\text{Er}^{3+}$  signal<sup>[70]</sup> with an asymmetric shape due to the overlapping  $\text{Er}4d_{3/2}$  and  $\text{Er}4d_{5/2}$  components. After annealing, the emission is still in the  $\text{Er}^{3+}$  region, but down to 5% of the initial value. The fact that the binding energy has not changed significantly speaks for a cage fusion with surviving  $\text{Er}_3\text{N}$  clusters instead of the cage cracking alternative. As the desorption of intact cages and the surface remainders seem not to add up to 100%, we have to conclude that a large fraction of the fullerenes decomposes and desorbs as small fragments.

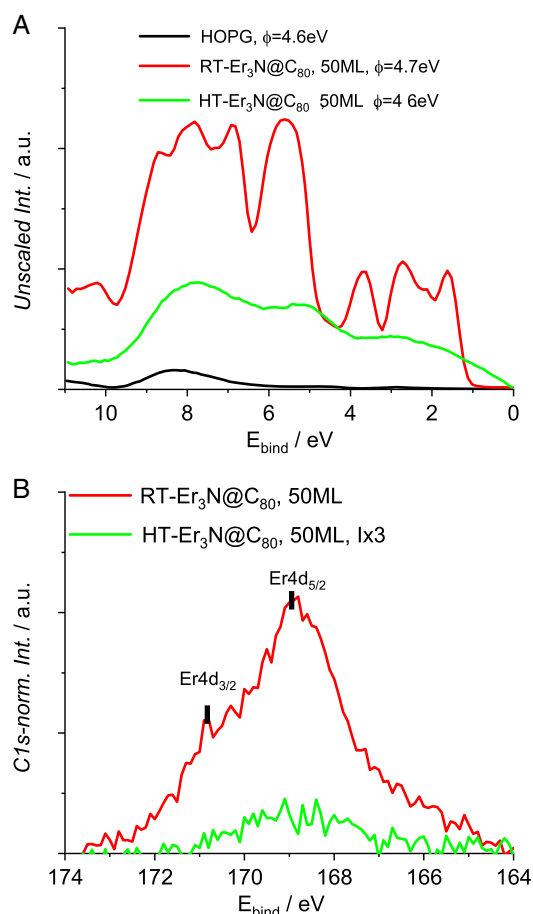


**Figure 8.** Photoelectron spectra of 50 ML  $\text{Er}_3\text{N}@C_{80}$  as-prepared (red) and after HT treatment (green). A) UPS in comparison with pure HOPG (black); B) XPS of the  $\text{Er}4d$  peak, intensity normalized with respect to the  $\text{C}1s$  emission, HT spectrum scaled by a factor of 3 for better visibility.

## 4. Conclusion

The analysis of high-purity  $\text{Er}_3\text{N}@C_{80}$  films has demonstrated that the LECBD method is also suitable for the growth of endohedral fullerene films. The growth mode differs from the empty IPR fullerene  $C_{60}$  most likely due to the higher dispersion interaction and the lower mobility of the cages. In the vibrational structure differences to other NCFs regarding the role of cluster movement could be demonstrated. Upon heating only a part of the fullerenes desorbs intactly, whereas another part remains on the surface forming chemically bound aggregates with some analogy to the behavior of non-IPR fullerenes.

## Supporting Information

Supporting Information is available from the Wiley Online Library or from the author.

## Acknowledgements

The authors thank Prof. Manfred M. Kappes for accompanying advice, Dr. Frank Hennrich for assistance with Raman spectra, Dr. Patrick Weis

for hints regarding the mass spectrometer handling, Holger Halberstadt and Klaus Stree for assistance regarding electronic issues and Dieter Waltz with his team for building the new ion source. All experiments were conducted at KIT. This work was funded by the DFG Center of Functional Nanostructures (CFN, subproject C4.6). J.W. acknowledges support of his new affiliation at Fraunhofer IAF during the final writing of this work.  
Open Access funding enabled and organized by Projekt DEAL.

## Conflict of Interest

The authors declare no conflict of interest.

## Data Availability Statement

The data that support the findings of this study are available from the corresponding author upon reasonable request.

## Keywords

atomic force microscopy, endohedral fullerenes, temperature programmed desorption spectroscopy, ultraviolet photoelectron spectroscopy, X-ray photoelectron spectroscopy

Received: October 23, 2020

Revised: December 21, 2020

Published online:

- 
- [1] S. Stevenson, G. Rice, T. Glass, K. Harich, F. Cromer, M. R. Jordan, J. Craft, E. Hadju, R. Bible, M. M. Olmstead, K. Maitra, A. J. Fisher, A. L. Balch, H. C. Dorn, *Nature* **1999**, 401, 55.
- [2] S. Stevenson, G. Rice, T. Glass, K. Harich, F. Cromer, M. R. Jordan, J. Craft, E. Hadju, R. Bible, M. M. Olmstead, K. Maitra, A. J. Fisher, A. L. Balch, H. C. Dorn, *Nature* **1999**, 402, 898.
- [3] E. B. Iezzi, J. C. Duchamp, K. Harich, T. E. Glass, H. M. Lee, M. M. Olmstead, A. L. Balch, H. C. Dorn, *J. Am. Chem. Soc.* **2002**, 124, 524.
- [4] S. Yang, T. Wei, F. Jin, *Chem. Soc. Rev.* **2017**, 46, 5005.
- [5] W. Krätschmer, L. Lamb, K. Fostiropoulos, D. Huffman, *Nature* **1990**, 347, 354.
- [6] M. M. Olmstead, A. de Bettencourt-Dias, J. C. Duchamp, S. Stevenson, H. C. Dorn, A. L. Balch, *J. Am. Chem. Soc.* **2000**, 122, 12220.
- [7] M. Waiblinger, K. Lips, W. Harneit, A. Weidinger, E. Dietel, A. Hirsch, *Phys. Rev. B* **2001**, 63, 045421.
- [8] M. Waiblinger, K. Lips, W. Harneit, A. Weidinger, E. Dietel, A. Hirsch, *Phys. Rev. B* **2001**, 64, 159901.
- [9] A. Stibor, H. Schefzyk, J. Fortágh, *Phys. Chem. Chem. Phys.* **2010**, 12, 13076.
- [10] J. Zhao, X. Huang, P. Jin, Z. Chen, *Coord. Chem. Rev.* **2015**, 289–290, 315.
- [11] A. Svitova, K. Braun, A. Popov, L. Dunsch, *ChemistryOpen* **2012**, 1, 207.
- [12] Z. Han, X. Wu, S. Roelle, C. Chen, W. P. Schiemann, Z. R. Lu, *Nat. Commun.* **2017**, 8, 692.
- [13] A. Tiwari, G. Dantelle, K. Porfyrakis, A. A. Watt, A. Ardavan, G. A. D. Briggs, *Chem. Phys. Lett.* **2008**, 466, 155.
- [14] M. Nie, J. Xiong, C. Zhao, H. Meng, K. Zhang, Y. Han, J. Li, B. Wang, L. Feng, C. Wang, T. Wang, *Nano Res.* **2019**, 12, 1727.
- [15] M. A. Jones, R. Taylor, A. Ardavan, K. Porfyrakis, G. Briggs, *Chem. Phys. Lett.* **2006**, 428, 303.
- [16] M. A. G. Jones, J. J. L. Morton, R. A. Taylor, A. Ardavan, G. A. D. Briggs, *Phys. Status Solidi B* **2006**, 243, 3037.
- [17] Y. Qi, A. F. Jarjour, X. Wang, R. A. Taylor, G. Zhang, *Opt. Commun.* **2009**, 282, 3637.
- [18] F. H. Hennrich, R. H. Michel, A. Fischer, S. Richard-Schneider, S. Gilb, M. M. Kappes, D. Fuchs, M. Bürk, K. Kobayashi, S. Nagase, *Angew. Chem. Int. Ed.* **1996**, 35, 1732.
- [19] T. Cummins, M. Bürk, M. Schmidt, J. Armbruster, D. Fuchs, P. Adelman, S. Schuppler, R. Michel, M. Kappes, *Chem. Phys. Lett.* **1996**, 261, 228.
- [20] H. J. Eisler, S. Gilb, F. H. Hennrich, M. M. Kappes, *J. Phys. Chem. A* **2000**, 104, 1762.
- [21] H. J. Eisler, F. H. Hennrich, S. Gilb, M. M. Kappes, *J. Phys. Chem. A* **2000**, 104, 1769.
- [22] C. R. Wang, T. Sugai, T. Kai, T. Tomiyama, H. Shinohara, *Chem. Commun.* **2000**, 557.
- [23] M. M. Olmstead, T. Zuo, H. C. Dorn, T. Li, A. L. Balch, *Inorg. Chim. Acta* **2017**, 468, 321.
- [24] M. M. Olmstead, T. Zuo, H. C. Dorn, T. Li, A. L. Balch, **2017**, CCDC entry 1541111, <https://doi.org/10.5517/ccdc.csd.cc1nqn89> (accessed: March 2019).
- [25] T. Akasaka, S. Nagase, K. Kobayashi, M. Wälchli, K. Yamamoto, H. Funasaka, M. Kako, T. Hoshino, T. Erata, *Angew. Chem. Int. Ed.* **1997**, 36, 1643.
- [26] A. A. Popov, L. Dunsch, *J. Am. Chem. Soc.* **2007**, 129, 11835.
- [27] S. Hu, P. Zhao, W. Shen, P. Yu, W. Huang, M. Ehara, Y. Xie, T. Akasaka, X. Lu, *Nanoscale* **2019**, 11, 13415.
- [28] R. M. Macfarlane, D. S. Bethune, S. Stevenson, H. C. Dorn, *Chem. Phys. Lett.* **2001**, 343, 229.
- [29] S. Stevenson, J. P. Phillips, J. E. Reid, M. M. Olmstead, S. P. Rath, A. L. Balch, *Chem. Commun.* **2004**, 24, 2814.
- [30] H. W. Kroto, *Nature* **1987**, 329, 529.
- [31] C. M. Beavers, M. N. Chaur, M. M. Olmstead, L. Echegoyen, A. L. Balch, *J. Am. Chem. Soc.* **2009**, 131, 11519.
- [32] T. Zuo, C. M. Beavers, J. C. Duchamp, A. Campbell, H. C. Dorn, M. M. Olmstead, A. L. Balch, *J. Am. Chem. Soc.* **2007**, 129, 2035.
- [33] F. Hennrich, E. Schneider, P. Weis, M. M. Kappes, *J. Am. Soc. Mass. Spectrom.* **2019**, 30, 1973.
- [34] Y. Sun, Y. Maeda, H. Sezaimaru, M. Sakaino, K. Kirimoto, *J. Appl. Phys.* **2014**, 116, 034301.
- [35] D. Löffler, S. S. Jester, P. Weis, A. Böttcher, M. M. Kappes, *J. Chem. Phys.* **2006**, 124, 054705.
- [36] D. Löffler, S. Ulas, S. S. Jester, P. Weis, A. Böttcher, M. M. Kappes, *Phys. Chem. Chem. Phys.* **2010**, 12, 10671.
- [37] J. Weippert, L. Hohmann, D. Strelnikov, P. Weis, M. L. Pop, A. Böttcher, M. M. Kappes, *J. Phys. Chem. C* **2019**, 123, 5721.
- [38] S. S. Jester, D. Löffler, P. Weis, A. Böttcher, M. M. Kappes, *Surf. Sci.* **2009**, 603, 1863.
- [39] A. Böttcher, P. Weis, A. Bihlmeier, M. M. Kappes, *Phys. Chem. Chem. Phys.* **2004**, 6, 5213.
- [40] P. Redhead, *Vacuum* **1962**, 12, 203.
- [41] H. Ulbricht, G. Moos, T. Hertel, *Phys. Rev. Lett.* **2003**, 90, 095501.
- [42] P. Deglmann, O. Treutler, H. Öhm, M. Häser, R. Ahlrichs, *Chem. Phys. Lett.* **1995**, 384, 103.
- [43] TURBOMOLE V7.4.1 2019, a development of University of Karlsruhe and Forschungszentrum Karlsruhe GmbH, 1989–2007, TURBOMOLE GmbH, since 2007, <http://www.turbomole.com>.
- [44] S. G. Balasubramani, G. P. Chen, S. Coriani, M. Diedenhofen, M. S. Frank, Y. J. Franzke, F. Furche, R. Grotjahn, M. E. Harding, C. Hättig, A. Hellweg, B. Helmich-Paris, C. Holzer, U. Huniar, M. Kaupp, A. Marefat Khah, S. K. Khani, T. Müller, F. Mack, B. D. Nguyen, S. M. Parker, E. Perlt, D. Rappoport, K. Reiter,

- S. Roy, M. Rückert, G. Schmitz, M. Sierka, E. Tapavicza, D. P. Tew, et al. *J. Chem. Phys.* **2020**, *152*, 184107.
- [45] A. Becke, *Phys. Rev. A* **1988**, *38*, 3098.
- [46] J. Perdew, *Phys. Rev. B* **1986**, *33*, 8822.
- [47] A. Schäfer, H. Horn, R. Ahlrichs, *J. Chem. Phys.* **1992**, *97*, 2571.
- [48] K. Eichkorn, O. Treutler, H. Öhm, M. Häser, R. Ahlrichs, *Chem. Phys. Lett.* **1995**, *240*, 283.
- [49] B. Kern, A. Böttcher, D. Strelnikov, *J. Phys. Chem. A* **2016**, *120*, 5868.
- [50] B. Kern, D. Strelnikov, P. Weis, A. Böttcher, M. M. Kappes, *J. Phys. Chem. A* **2013**, *117*, 8251.
- [51] D. Rappoport, F. Furche, *J. Chem. Phys.* **2007**, *126*, 201104.
- [52] H. Liu, P. Reinke, *J. Chem. Phys.* **2006**, *124*, 164707.
- [53] A. Böttcher, P. Weis, S. S. Jester, D. Löffler, A. Bihlmeier, W. Klopper, M. M. Kappes, *Phys. Chem. Chem. Phys.* **2005**, *7*, 2816.
- [54] P. A. Graviil, M. Devel, P. Lambin, X. Bouju, C. Girard, A. A. Lucas, *Phys. Rev. B* **1996**, *53*, 1622.
- [55] C. Nörenberg, D. F. Leigh, D. Cattaneo, K. Porfyrakis, A. L. Bassi, C. S. Casari, M. Passoni, J. H. G. Owen, G. A. D. Briggs, *J. Phys.: Conf. Ser.* **2008**, *100*, 052080.
- [56] S. Schimmel, Z. Sun, D. Baumann, D. Krylov, N. Amoylova, A. Popov, B. Büchner, C. Hess, *Nanotechnology* **2017**, *8*, 1127.
- [57] T. Kawase, H. Kurata, *Chem. Rev.* **2006**, *106*, 5250.
- [58] D. Lichtenberger, K. Nebesny, C. Ray, D. Huffman, L. Lamb, *Chem. Phys. Lett.* **1991**, *176*, 203.
- [59] H. Shiozawa, H. Rauf, T. Pichler, D. Grimm, X. Liu, M. Knupfer, M. Kalbac, S. Yang, L. Dunsch, B. Büchner, D. Batchelor, *Phys. Rev. B* **2005**, *72*, 195409.
- [60] S. Yang, L. Dunsch, *J. Phys. Chem. B* **2005**, *109*, 12320.
- [61] C. Tang, W. Zhu, K. Deng, *Acta Chim. Sin.* **2009**, *67*, 1421.
- [62] A. D. Becke, *Phys. Rev. A* **1988**, *38*, 3098.
- [63] C. Lee, W. Yang, R. G. Parr, *Phys. Rev. B* **1988**, *37*, 785.
- [64] Y. Inada, H. Orita, *J. Comput. Chem.* **2008**, *29*, 225.
- [65] M. Krause, H. Kuzmany, P. Georgi, L. Dunsch, K. Vietze, G. Seifert, *J. Chem. Phys.* **2001**, *115*, 6596.
- [66] M. Krause, J. Noack, R. Marczak, P. Georgi, L. Dunsch, *AIP Conf. Proc.* **2003**, *685*, 50.
- [67] L. Dunsch, M. Krause, J. Noack, P. Georgi, *J. Phys. Chem. Solids* **2004**, *65*, 309.
- [68] S. Yang, S. I. Troyanov, A. A. Popov, M. Krause, L. Dunsch, *J. Am. Chem. Soc.* **2006**, *128*, 16733.
- [69] D. Löffler, N. Bajales, M. Cudaj, P. Weis, S. Lebedkin, A. Bihlmeier, D. P. Tew, W. Klopper, A. Böttcher, M. M. Kappes, *J. Chem. Phys.* **2009**, *130*, 164705.
- [70] T. Miyazaki, R. Sumii, H. Umamoto, H. Okimoto, Y. Ito, T. Sugai, H. Shinohara, T. Zaima, H. Yagi, S. Hino, *Chem. Phys.* **2012**, *397*, 87.